Gold-embedded zigzag graphene nanoribbons as spin gapless semiconductors

Xiaohui Hu,[1] Wei Zhang,[2] Litao Sun,[1,*] and Arkady V. Krasheninnikov[3,4]

[1]*SEU-FEI Nano-Pico Center, Key Lab of MEMS of Ministry of Education, Southeast University, 210096 Nanjing, China*

[2]*Shanghai Institute of Applied Physics, Chinese Academy of Sciences, 201800 Shanghai, China*

[3]*Department of Physics, University of Helsinki, FI-00014 Helsinki, Finland*

[4]*Department of Applied Physics, Aalto University, FI-00076 Aalto, Finland*

(Received 13 June 2012; revised manuscript received 12 October 2012; published 15 November 2012)

Using density-functional theory calculations, we studied the electronic and magnetic properties of zigzag graphene nanoribbons (ZGNRs) with gold (Au) atoms embedded into different sites of the ZGNRs. Strong site dependence was found, and the system had the ferromagnetic or antiferromagnetic ground state depending on the Au atom position. Spin gapless semiconductor (SGS) behavior was observed when the Au atom was embedded into the center and edge sites of the ZGNRs. The simulations showed that the electronic structure of the ribbon strongly depends on ZGNR width, but the SGS behavior is always present when the Au atom is embedded into the center and edge sites. The SGS properties were also found to be dependent on impurity atom concentration, so that they can be tuned by either selecting the proper positions of Au atoms or changing their concentration. Our results suggest a flexible way of designing SGSs, which could be used in various spintronic, electronic, and optoelectronic applications.

DOI: 10.1103/PhysRevB.86.195418 PACS number(s): 73.22.Pr, 61.48.Gh, 81.05.ue

I. INTRODUCTION

Recently, the new concept of SGS[1] has been proposed by Wang, who analyzed the electronic properties of doped $PbPdO_2$ systems using first-principles calculations. The SGS materials have unique band structures. The top of the valence band of one spin channel and the bottom of the conduction band of at least one spin channel touch at the Fermi level. According to possible band structure configurations, four typical kinds of SGS have been defined.[1] For the first case, one spin channel is gapless, while the other spin channel is semiconducting. In the second case, there is a gap between the conduction and valence bands for both the spin-up and spin-down electrons, while there is no gap between the spin-up electrons in the valence band and the spin-down electrons in the conduction band. In the third case, one spin channel is gapless, and the other spin channel is semiconducting, with the top of the valence band being lower than the Fermi level. In the fourth case, one spin channel is gapless, while the bottom of the conduction band for the other spin channel touches the Fermi level, which is separated from its corresponding valence band by a gap.

The SGS materials have more interesting features than the conventional semiconductors.[2,3] For example, no energy is required to excite electrons from the valence band to the conduction band, while the density of states at the Fermi level is zero, and both electrons and holes can be 100% spin polarized at the Fermi level, which is the most desirable property of semiconductors in spintronics. Due to these features, the SGSs are expected to be very sensitive to external influences. Indeed, unusually strong electroresistance and magnetoresistance effects have been experimentally observed in doped $PbPdO_2$ thin films.[2]

Graphene,[4] a single atomic layer of graphite, is a promising candidate material for next-generation electronics. Pure graphene is a gapless semiconductor with linear band energy dispersion and a high mobility of charge carriers.[5] The electronic and magnetic properties of graphene doped with metal atoms have been extensively studied.[6,7] Given the gapless band structure and linear dispersion of graphene, SGSs can be designed from graphene-based materials via either chemical doping or application of external pressure.

Graphene nanoribbons (GNRs), one-dimensional structures made from graphene, have also been experimentally realized.[8–10] According to edge geometries, GNRs can be designed as zigzag or armchair GNRs. ZGNRs have two of the most stable spin configurations, one with the spins at both edges being ferromagnetically (FM) coupled; another is that the spins are coupled antiferromagnetically (AFM). The AFM configuration is more stable than the FM one. It has been shown that the ferromagnetic ZGNRs are metallic, but the antiferromagnetic ZGNRs are semiconducting.[11–13] ZGNRs are known to have special localized edge states, which are AFM coupled between the two edges.[14–16] Recent experiment has revealed the presence of the edge states in ZGNRs.[17] However, the edge states are easily destroyed by several mechanisms, such as edge reconstructions, edge passivation, and edge closure.[18] The effects of edge disorder and deformation on the GNRs have also been studied.[19,20] In the presence of impurities, the edge states could be changed to ferromagnetic alignment.[21] The strong impurity site dependence of GNRs behavior has been observed, including transport[22,23] and magnetic properties.[24] Several studies have also addressed atom doping of GNRs with metal[25–28] and N atoms.[29] Interestingly, the SGS behavior has been found in ZGNRs with nitrogen doping at the edge,[29] and in boron nitride nanoribbons with vacancies.[30]

Graphene with embedded Au atoms has been experimentally manufactured, as revealed by transmission electron microscopy studies.[31] Motivated by the experimental progress, in this work we study electronic and magnetic properties of ZGNRs with Au atoms embedded using density-functional theory (DFT) calculations. Strong site dependence of the electronic structure was observed, and the system possessed a ferromagnetic or antiferromagnetic ground state depending on the Au atom position. SGS behavior was observed when the Au atom was embedded into the center and edge sites of

ZGNRs. Our results provide a flexible way of designing SGS based on Au embedded ZGNRs (Au-ZGNRs), which could open up a new direction for practical spintronic applications.

II. METHOD AND MODEL

Calculations were performed using the Vienna *ab initio* simulation package (VASP) code[32,33] based on DFT. The generalized gradient approximation (GGA) with the Perdew-Burke-Ernzerhof (PBE) parametrization[34] was chosen for the exchange-correlation functional. The core electrons were accounted for within the projector augmented wave (PAW) approach.[35,36] The plane wave cutoff energy was set to 500 eV, because a higher value had little effect on the results. The structures were relaxed until the energy and the force on each atom were less than 10^{-5} eV and 0.01 eV/Å, respectively. A $15 \times 1 \times 1$ k-point mesh with Monkhorst-Pack scheme was used for sampling the one-dimension (1D) Brillouin zone. To simulate the isolated ribbons, the intervals among the ribbons were maintained at 20 Å for both layer-layer and edge-edge distances. Most calculations were performed for a supercell containing four unit cells.

Following the established convention,[37] the ZGNRs were characterized by the number of zigzag chains (N) across the ribbon width. We chose a ZGNR with $N = 8$ as the typical system. The edge carbon (C) atoms were all saturated by hydrogen atoms to avoid dangling bonds. Double vacancy doping was implemented by deleting a pair of C atoms and adding the Au atom in the middle of the four nearest neighboring C atoms. There are two kinds of doping sites of an Au atom on the ZGNR. One is that an Au atom replaces two adjacent C atoms with the bond oriented perpendicular to the ZGNR axis, as indicated by the magenta ellipses in Fig. 1(a). Another is that an Au atom replaces two adjacent C atoms with the bond being diagonal to the ZGNR axis, as indicated by the blue ellipses in Fig. 1(a). The symbols A to G denote different substitutional sites, A to D corresponding to the perpendicular bonds, and E to G relevant to the diagonal bonds. Accordingly, the Au atom embedded ZGNRs can be named as Au-A-ZGNR, Au-B-ZGNR, Au-C-ZGNR, and Au-D-ZGNR, etc. Figure 1(b) illustrates the equilibrium structure of an Au atom embedded into the A vacancy site. The Au atom is located in the C plane, forming four covalent bonds with the nearest neighboring C atoms. The Au-C bond length was 1.98 Å, in agreement with previous calculations.[28]

III. RESULTS AND DISCUSSION

A. Electronic and magnetic properties of the Au-ZGNRs with gold atoms at different sites

To get insight into the preferential positions of the Au atom and assess the relative stability of Au-ZGNRs, we calculated binding energy E_b of Au atoms to the ZGNR, which is defined as the sign reversed difference between the energy of the ribbon with the Au atom in the substitutional position and the energy of the reconstructed double vacancy plus the energy of the isolated Au atom. Figure 2(a) presents E_b for different sites in the ZGNR. Comparing E_b of the seven structures we studied, it is evident that the perpendicular bond sites are energetically more favorable than the diagonal ones. For the perpendicular bond sites from A to D, the middle positions are more stable than the edge ones. To confirm the structural stability of the Au-ZGNRs, taking Au-D-ZGNR as an example, we carried out DFT-based molecular dynamics (MD) simulation in the canonical ensemble.[38,39] The total simulation time was 5 ps and the time step is set at 1 fs. During the MD simulation we do not observe any signs of structure disruption even at a high temperature of 1000 K. A snapshot of Au-D-ZGNR at the simulation time 5 ps is displayed in Fig. 2(b). The MD results indicate that Au-D-ZGNR should be stable at room temperature. Taking into account the energetic of the ribbons with embedded Au atoms, in what follows, we concentrate on the structures with perpendicular bond sites.

According to previous theoretical studies, the pristine ZGNR has AFM ground state, with electron magnetic moments FM ordered along the same edge and AFM coupled between the opposite edges. The AFM ground state of the pristine ZGNR may change upon embedding foreign atoms. To determine the ground state of the Au-ZGNRs at different sites, AFM coupled, FM coupled, and nonmagnetic (NM) states were considered. The relative energies of different magnetic configurations are given in Table I. The magnetic states are found to be more stable than the NM one. For Au-A-ZGNR, Au-B-ZGNR, and Au-C-ZGNR structures, the FM states are more stable as compared to their corresponding AFM states, indicating that the FM configurations are their ground states. For the Au-D-ZGNR structure, the AFM state is 4 meV lower than the FM state, displaying the AFM ground state. Depending on the Au atom position at different embedded sites, the ground state of the system can be AFM or FM.

To get insight into the magnetic properties of ZGNRs with an Au atom embedded into different sites, the ground state spin-density distributions of the four configurations are

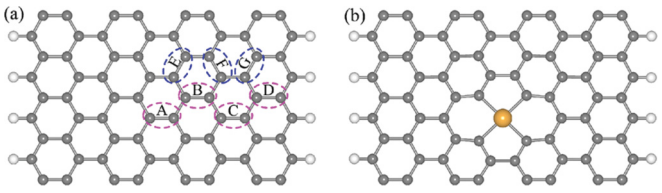

FIG. 1. (Color online) (a) Atomic structure of a ZGNR. Symbols A to G denote different substitutional sites. (b) Structural model of Au-A-ZGNR. The white, gray, and yellow balls are hydrogen, carbon, and gold atoms, respectively.

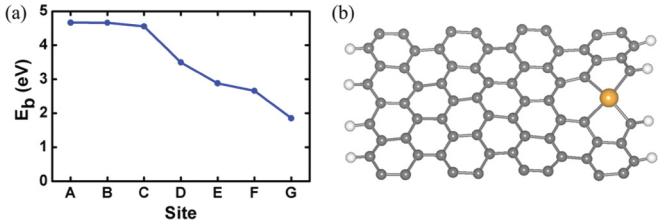

FIG. 2. (Color online) (a) Binding energy E_b of Au atoms to the ZGNR at different sites. (b) A snapshot of Au-D-ZGNR taken after 5 ps of DFT-MD simulations at temperature of 1000 K.

TABLE I. Relative energies ΔE (in meV) of different magnetic phases of Au-ZGNRs at different sites, along with the total spin magnetic moment M (in μ_B), the magnetic moment of the Au atom, and the average magnetic moments of the left edge C atoms and the right edge C atoms.

	$E_{NM}-E_{AFM}$	$E_{NM}-E_{FM}$	M	Au	C_L	C_R
Au-A-ZGNR	233	261	2.78	0.04	0.25	0.25
Au-B-ZGNR	230	257	2.80	0.04	0.25	0.25
Au-C-ZGNR	198	227	2.58	0.04	0.25	0.23
Au-D-ZGNR	132	128	0.99	−0.02	0.25	−0.05

presented in Fig. 3. Figure 3(a) shows the spin density of the FM Au-A-ZGNR, which is mostly localized on the two edges and decays towards the middle of the ribbon. The FM Au-A-ZGNR is found to have a magnetic moment of 2.78 μ_B, higher than that of pristine FM 8-ZGNR (2.09 μ_B). This higher magnetic moment can be attributed to electron transfer from the Au atom to neighboring C atoms, which induces a magnetic moment on both Au and C atoms. The magnetic moment of the C atoms around the Au atom is obviously greater than that of the other C atoms in the corresponding site, as shown in Fig. 3(a). However, the magnetic moments of the two edge C atoms are less affected. The Au-B-ZGNR exhibits a behavior similar to the Au-A-ZGNR, and has a total magnetic moment of 2.80 μ_B. The net magnetic moment of the Au-C-ZGNR is 2.58 μ_B, smaller than those of the Au-A-ZGNR and Au-B-ZGNR. Apparently, an Au atom embedded at the C site induces spin suppression on the edge close to the Au atom. In contrast, the magnetic moment of the right edge C atom nearest to the Au atom increases because of charge transfer from the Au atom. The spin density of the AFM Au-D-ZGNR is displayed in Fig. 3(d). The spins on the doped edge are strongly suppressed, and the system has a magnetic moment of 0.99 μ_B. Pristine AFM ZGNR has a zero net magnetic moment. Au doping at the edge suppresses the magnetic moment on that edge and destroys the symmetry of spin distributions, consequently inducing the magnetic moment. In previous studies,[40] edge defects and impurities were found to have a similar effect on the magnetic structure of the ribbons.

Figures 4(a) to 4(d) show the spin-polarized band structures of ZGNRs with the Au atom embedded into different sites

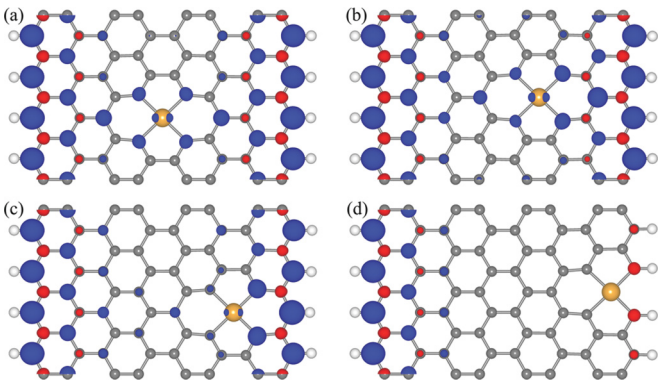

FIG. 3. (Color online) Spin densities of (a) FM Au-A-ZGNR, (b) FM Au-B-ZGNR, (c) FM Au-C-ZGNR, and (d) AFM Au-D-ZGNR. The isovalues for the blue and red isosurfaces were 0.004 and −0.004 $e/\text{Å}^3$, respectively.

from the center to the edge of the ribbon. All the bands, especially those near the Fermi level, are obviously spin polarized, as directly induced by the embedded Au atom. The FM Au-A-ZGNR shows a semiconducting character for each spin channel; the band gaps are 0.19 and 0.42 eV for spin-up and spin-down channels, respectively, as shown in Fig. 4(a). Interestingly, the valence band maximum of the spin-up channel touches the Fermi level at the X point, whereas the conduction band minimum (CBM) of the spin-down channel touches the Fermi level at the Γ point. Therefore, the band is indirectly gapless, which means that Au-A-ZGNR is a typical SGS and belongs to the second case defined by Wang.[1] Upon the Au atom embedding at the B site, the bands become very similar with those in Fig. 4(a), and the semiconducting character is well preserved for both spin channels. The band gaps are 0.25 and 0.44 eV for spin-up and spin-down channels, respectively, as illustrated in Fig. 4(b). Figure 3(b) clearly shows that the electron density around the Au atom does not exhibit any evident change. Hence, the system displays an SGS character similar to the Au-A-ZGNR. Upon moving the Au atom further to the C site, the spin-up channel remains semiconducting with a gap of 0.29 eV, whereas the spin-down CBM shifts down across the Fermi level and becomes metallic, Fig. 4(c). Therefore, the FM Au-C-ZGNR is half-metallic. For the AFM Au-D-ZGNR, where the Au atom is embedded at the edge site of the ribbon, spin-up channel shows a semiconducting characteristic with a band gap of 0.21 eV. The spin-down channel has a tiny gap, only 0.05 eV. According to Wang,[41] the term "gapless" is used for an energy gap that is approximately 0.1 eV or smaller than 0.1 eV. So for the Au-D-ZGNR, another kind of SGS systems is predicted, which belongs to the fourth case. Overall, our results reveal that SGS and half-metal properties are obtained via an Au atom doping at different sites.

As DFT calculations with the GGA functional normally underestimate the band gap of semiconductors, and the SGS behavior is sensitive to the band structure details around the Fermi energy, we performed test calculations with the hybrid HSE06 functional,[42–44] which could give more reliable results. Taking the Au-D-ZGNR as an example, we found that the spin-up gap and spin-down gap increase to 0.51 and 0.06 eV, respectively, but the system remains to be SGS, confirming our results.

Figures 4(e) to 4(h) show the corresponding charge densities of band a (indicated by black arrows) at the Gamma point, named Γ state. The charge densities indicate that the Γ state mainly comes from the Au atom and the neighboring C atoms in all cases. For Au-A-ZGNR and Au-B-ZGNR, a

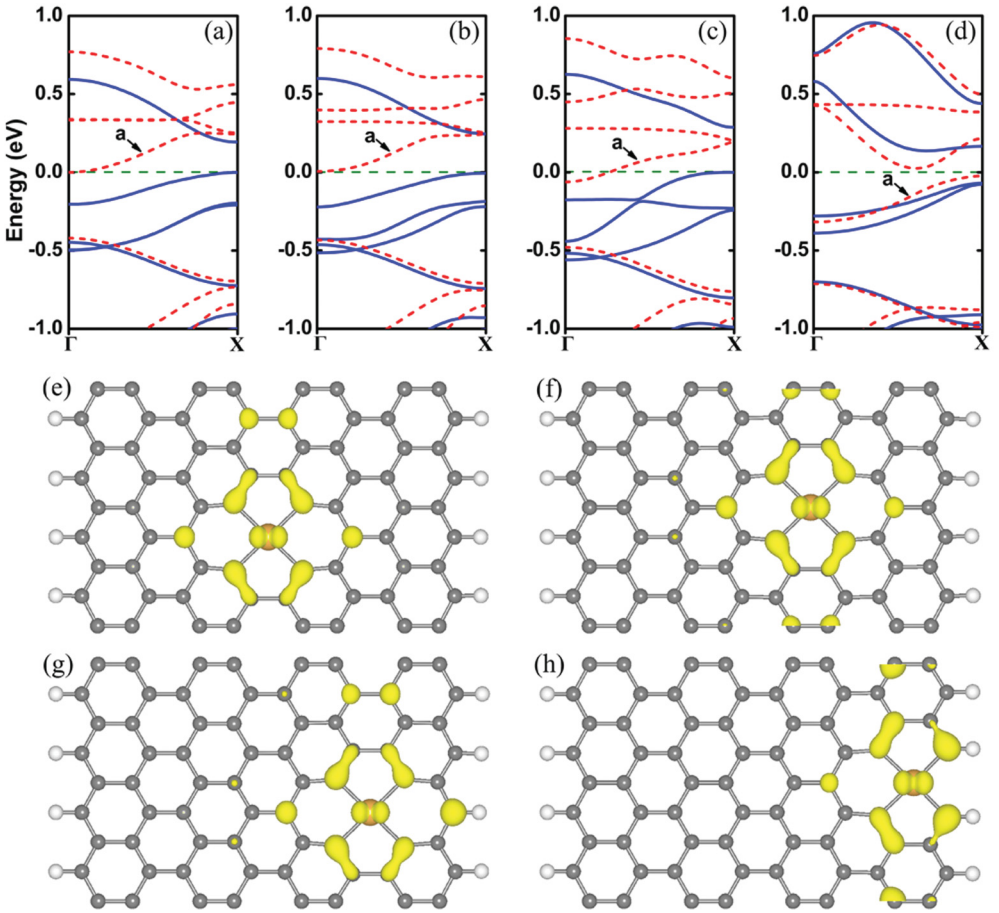

FIG. 4. (Color online) Band structures of (a) FM Au-A-ZGNR, (b) FM Au-B-ZGNR, (c) FM Au-C-ZGNR, and (d) AFM Au-D-ZGNR. The corresponding charge densities of band a (indicated by black arrows) at the Gamma point (Γ) are shown in (e), (f), (g), and (h). The blue solid line and red dashed line denote spin-up and spin-down channels, respectively. The Fermi level is denoted by a horizontal olive dashed line. The isovalue is set to be 0.003 $e/\text{Å}^3$.

significant part of the Γ state comes from the inner C atoms, and nothing from the edge C atoms of the ribbon. However, for Au-C-ZGNR and Au-D-ZGNR, both inner and edge C atoms contribute. Therefore, the variations in band structures caused by the embedded Au atom into different ZGNR sites can be attributed to the interaction between the Au atom and the edge C atoms. The electron charge transferred from the Au atom to ZGNRs is calculated to be 0.69, 0.69, 0.72 and 0.70 e from the center site to edge site. The transferred charge corresponds to the lowest unoccupied edge states. For example, when the Au atom is embedded into the center site, the electrons occupy both left and right edge states evenly, while for the edge site, the electrons prefer to occupy the state in the same edge due to Coulomb interaction between the Au atom and ZGNR. So the interaction between the Au atom and ZGNRs is strongest at the edge and weakest in the center of the ribbon. This situation is similar to that of an alkali metal adsorbed on ZGNRs.[45] As the Au atom is moved closer to the edge, the interaction between the Au atom and edge C atoms becomes stronger. Consequently, band a shifts down, crossing the Fermi level [Fig. 4(c)] until reaching the valence band [Fig. 4(d)].

To further analyze the electronic structure of the Au-ZGNRs at different sites, we calculated the total and projected density of states (TDOS and PDOS, respectively) of these systems. The densities of states of these systems are shown in Fig. 5. In each panel, the top plot is the TDOS, the next is the PDOS of the Au atom, below it is the PDOS of the left edge C atom (C_L), and the bottom plot is the PDOS of the right edge C atom (C_R). For the ZGNRs with the Au atom embedded into the center site, such as Au-A-ZGNR, the transferred electron charge evenly occupies both left and right edge states. As a result, the PDOSs of the two edge C atoms are equally perturbed, but only to a small extent. For sufficiently wide ZGNRs, the influence on the edge states is negligible. The PDOS of the Au-B-ZGNR is similar to that of the Au-A-ZGNR. For the Au-C-ZGNR, the effect on the left edge states weakens, whereas that on the right edge states strengthens. For the Au-D-ZGNR, the PDOS of C_L is not affected, whereas the Au atom and C_R are strongly hybridized around the Fermi level, destroying the edge states from C_R. These results indicate that the embedding of Au atoms into different sites drastically modifies the electronic structure of ZGNRs.

B. Dependence of the electronic properties on ribbon width

To test the dependence of the electronic properties on ribbon width, we have calculated the electronic structure of

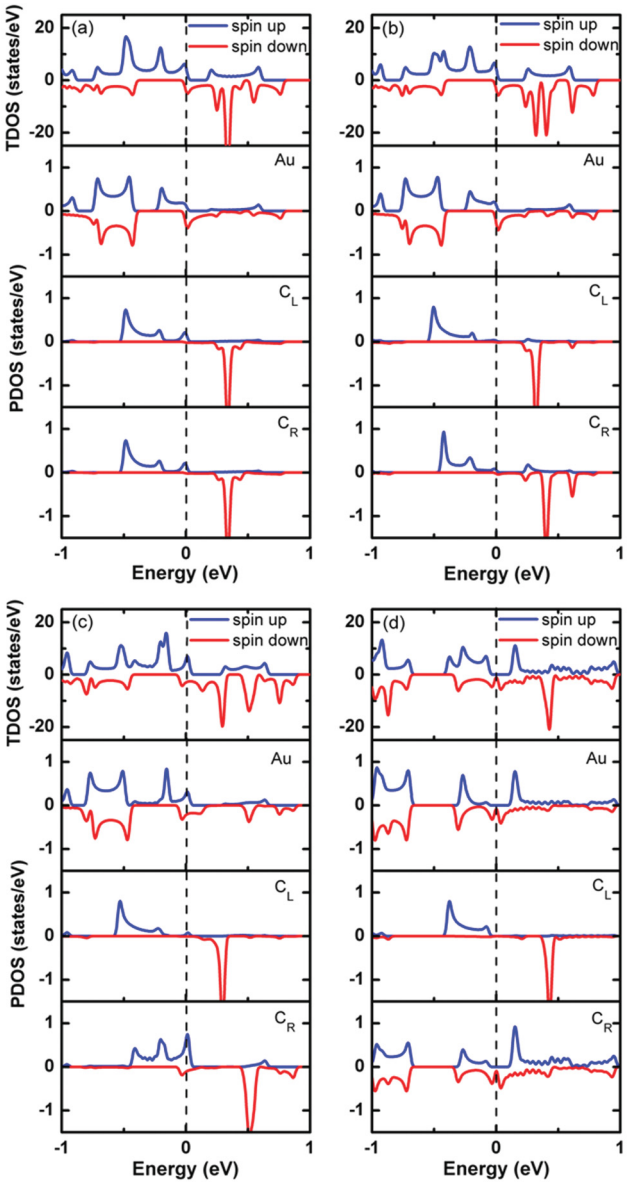

FIG. 5. (Color online) Total and projected densities of states (TDOS/PDOS) of (a) FM Au-A-ZGNR, (b) FM Au-B-ZGNR, (c) FM Au-C-ZGNR, and (d) AFM Au-D-ZGNR. The blue and red lines indicate spin-up and spin-down channels. The top panel is the TDOS, the next is the PDOS for the Au atom, below it is the PDOS of the left edge C atom (C_L), and the bottom one is the PDOS of the right edge C atom (C_R).

a series of Au-ZGNRs with different widths and various sites where the Au atom was embedded, including the center and edge sites. The results are presented in Table II. For the center-site-embedded Au-ZGNRs, all the systems possess the FM ground state. With the increase of the ribbon width, center-site Au-ZGNRs can be tuned from metal to SGS and then to metal. This width dependence can be explained by the interaction between the Au atom and the edge C atoms, which becomes weaker and weaker as ribbon width increases. This suggests that SGS behavior can be induced by adjusting the width of ribbon appropriately. However, for edge-site-embedded Au-ZGNRs, all the systems have the AFM ground

TABLE II. Spin up gap (Δ_α), spin down gap (Δ_β), and the electronic character (EC) of Au-ZGNR with different width N. $N(c)$ and $N(e)$ stand for center-site and edge-site embedded ZGNR (M denotes metal; SGS stands for spin gapless semiconductor).

$N(c)$	Δ_α(eV)	Δ_β(eV)	EC	$N(e)$	Δ_α(eV)	Δ_β(eV)	EC
6	0	0	M	6	0.22	0.10	SGS
7	0	0	M	7	0.21	0.07	SGS
8	0.19	0.42	SGS	8	0.21	0.05	SGS
9	0.15	0.41	SGS	9	0.21	0.04	SGS
10	0.08	0.40	SGS	10	0.20	0.03	SGS
11	0.03	0.39	SGS	11	0.20	0.03	SGS
12	0	0.38	M	12	0.20	0.02	SGS
13	0	0.38	M	13	0.20	0.02	SGS
14	0	0.37	M	14	0.20	0.02	SGS

state. Surprisingly, different from center-site case, all edge-site Au-ZGNRs display the SGS behavior independent of ribbon width, which also indicates that the interaction between the Au atom and the edge C atoms does not change. Accordingly, one could obtain SGS by selecting proper position of the impurity atom and width of the system.

C. Dependence of the electronic properties on dopant atom concentration

Taking the center-site embedded Au-ZGNR as an example, we further investigated the effects of doping concentration on the band structures. Here the doping concentration is tuned by changing the length of the ZGNR. We used the number of unit cells in the supercell to study different dopant atom concentrations, denoted as Au-4ZGNR for the model structure shown in Fig. 1(a). Figure 6 gives the band structures of the Au atom embedded at the center site of ZGNR for different dopant atom concentrations of Au-3ZGNR, Au-4ZGNR and Au-5ZGNR, respectively. All three cases present the FM ground state. For the Au-3ZGNR corresponding to a higher concentration of dopant atoms, the system demonstrates a metal character; while for the lower concentration Au-5ZGNR, the system is a half-metal. The SGS only appears for Au-4ZGNR. So the electronic structure is sensitive to the dopant atom concentration. With decreasing Au atom concentration,

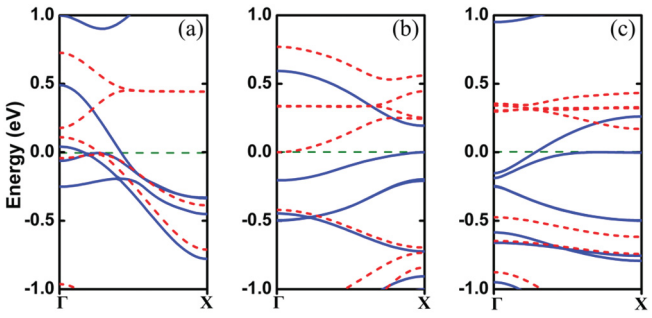

FIG. 6. (Color online) Band structures of (a) Au-3ZGNR, (b) Au-4ZGNR, and (c) Au-5ZGNR corresponding to different dopant atom concentrations. The blue solid line and red dashed line denote to the spin-up and spin-down channels, respectively. The Fermi level is marked by a horizontal olive dashed line.

the interaction between the adjacent Au atoms weakens. This gives rise to a decrease in energy dispersion of the impurity bands, explaining the metal bands in Au-3ZGNR but half-metal in Au-5ZGNR. Our calculations show that Au-6ZGNR has the AFM ground state. It is known that the pristine ZGNR has the AFM ground state, so we expect that in the limit of the Au atom in an infinite ZGNR, the edges would revert to the AFM alignment, and the electronic structure of Au-ZGNRs will converge to that of the pristine ZGNRs. The results exhibit that the doping concentration is important for obtaining SGS. So a proper position and an appropriate doping concentration would be the key factors to realize SGS in this system.

IV. CONCLUSION

In summary, the electronic and magnetic properties of ZGNRs embedded with Au atoms into double vacancies at different sites were studied using DFT calculations. The system possesses the FM or AFM ground state depending on the Au atom position. The SGS behavior was observed when the Au atom was embedded into the center and edge sites of the ZGNRs. The electronic structure of the ribbon strongly depends on ZGNR width, but the SGS behavior is always present when the Au atom is embedded into the center and edge sites. The SGS properties also depend on impurity atom concentration, so that they can be tuned by either selecting the proper positions of Au atoms or changing their concentration. Our results points towards a new route to the design of SGSs, which could be used in various spintronic, electronic, and optoelectronic applications.

ACKNOWLEDGMENTS

This work was supported by the National Basic Research Program of China (Grants No. 2011CB707601 and No. 2009CB623702), the National Natural Science Foundation of China (Grants No. 51071044, No. 60976003, and No. 61006011), Program for New Century Excellent Talents in University (NCEF-09-0293), Specialized Research Fund for the Doctoral Program of Higher Education (20100092110014), and Open Research Fund of State Key Laboratory of Bioelectronics. A.V.K. acknowledges support from the Academy of Finland through projects 130852, 218545, and 263416. W.Z. acknowledges the support from Strategically Leading Program of the Chinese Academy of Sciences (Grant No. XDA02040100) and the National Natural Science Foundation of China (Grants No. 11075196 and No. 11005142).

*Corresponding author: slt@seu.edu.cn

[1] X. L. Wang, Phys. Rev. Lett. **100**, 156404 (2008).
[2] X. L. Wang, G. Peleckis, C. Zhang, H. Kimura, and S. X. Dou, Adv. Mater. **21**, 2196 (2009).
[3] X. L. Wang, S. X. Dou, and C. Zhang, NPG Asia Mater. **2**, 31 (2010).
[4] A. K. Geim and K. S. Novoselov, Nat. Mater. **6**, 183 (2007).
[5] A. H. Castro Neto, F. Guinea, N. M. R. Peres, K. S. Novoselov, and A. K. Geim, Rev. Mod. Phys. **81**, 109 (2009).
[6] A. V. Krasheninnikov, P. O. Lehtinen, A. S. Foster, P. Pyykko, and R. M. Nieminen, Phys. Rev. Lett. **102**, 126807 (2009).
[7] E. J. G. Santos, A. Ayuela, and D. Sánchez-Portal, New J. Phys. **12**, 053012 (2010).
[8] L. Tapasztó, G. Dobrik, P. Lambin, and L. P. Biró, Nat. Nanotechnol. **3**, 397 (2008).
[9] M. Y. Han, B. Özyilmaz, Y. B. Zhang, and P. Kim, Phys. Rev. Lett. **98**, 206805 (2007).
[10] Z. H. Chen, Y. M. Lin, M. J. Rooks, and P. Avouris, Physica E **40**, 228 (2007).
[11] Y. W. Son, M. L. Cohen, and S. G. Louie, Phys. Rev. Lett. **97**, 216803 (2006).
[12] L. Yang, C. H. Park, Y. W. Son, M. L. Cohen, and S. G. Louie, Phys. Rev. Lett. **99**, 186801 (2007).
[13] W. Y. Kim and K. S. Kim, Nat. Nanotechnol. **3**, 408 (2008).
[14] K. Nakada, M. Fujita, G. Dresselhaus, and M. S. Dresselhaus, Phys. Rev. B **54**, 17954 (1996).
[15] M. Fujita, K. Wakabayashi, K. Nakada, and K. Kusakabe, J. Phys. Soc. Jpn. **65**, 1920 (1996).
[16] H. Lee, Y. W. Son, N. Park, S. Han, and J. Yu, Phys. Rev. B **72**, 174431 (2005).
[17] C. Tao, L. Jiao, O. V. Yazyev, Y.-C. Chen, J. Feng, X. Zhang, R. B. Capaz, J. M. Tour, A. Zettl, S. G. Louie, H. Dai, and M. F. Crommie, Nat. Phys. **7**, 616 (2011).
[18] J. Kunstmann, C. Özdoğan, A. Quandt, and H. Fehske, Phys. Rev. B **83**, 045414 (2011).
[19] E. R. Mucciolo, A. H. Castro Neto, and C. H. Lewenkopf, Phys. Rev. B **79**, 075407 (2009).
[20] X. H. Hu, L. T. Sun, and A. V. Krasheninnikov, Appl. Phys. Lett. **100**, 263115 (2012).
[21] J. Park, H. Yang, K. S. Park, and E.-K. Lee, J. Chem. Phys. **130**, 214103 (2009).
[22] B. Biel, X. Blase, F. Triozon, and S. Roche, Phys. Rev. Lett. **102**, 096803 (2009).
[23] E. Cruz-Silva, Z. M. Barnett, B. G. Sumpter, and V. Meunier, Phys. Rev. B **83**, 155445 (2011).
[24] S. R. Power, V. M. de Menezes, S. B. Fagan, and M. S. Ferreira, Phys. Rev. B **84**, 195431 (2011).
[25] W. H. Brito and R. H. Miwa, Phys. Rev. B **82**, 045417 (2010).
[26] V. A. Rigo, T. B. Martins, A. J. R. daSilva, A. Fazzio, and R. H. Miwa, Phys. Rev. B **79**, 075435 (2009).
[27] R. C. Longo, J. Carrete, and L. J. Gallego, J. Chem. Phys. **134**, 024704 (2011).
[28] W. Zhang, L. T. Sun, Z. J. Xu, A. V. Krasheninnikov, P. Huai, Z. Y. Zhu, and F. Banhart, Phys. Rev. B **81**, 125425 (2010).
[29] Y. F. Li, Z. Zhou, P. W. Shen, and Z. F. Chen, ACS Nano **3**, 1952 (2009).
[30] Y. F. Pan and Z. Q. Yang, Phys. Rev. B **82**, 195308 (2010).
[31] Y. Gan, L. Sun, and F. Banhart, Small **4**, 587 (2008).
[32] G. Kresse and J. Furthmüller, Comput. Mater. Sci. **6**, 15 (1996).
[33] G. Kresse and J. Furthmüller, Phys. Rev. B **54**, 11169 (1996).
[34] J. P. Perdew, K. Burke, and M. Ernzerhof, Phys. Rev. Lett. **77**, 3865 (1996).
[35] P. E. Blöchl, Phys. Rev. B **50**, 17953 (1994).
[36] G. Kresse and D. Joubert, Phys. Rev. B **59**, 1758 (1999).
[37] F. Cervantes-Sodi, G. Csányi, S. Piscanec, and A. C. Ferrari, Phys. Rev. B **77**, 165427 (2008).

[38]Z. H. Zhang and W. L. Guo, J. Am. Chem. Soc. **131**, 6874 (2009).
[39]Z. H. Zhang, X. J. Wu, W. L. Guo, and X. C. Zeng, J. Am. Chem. Soc. **132**, 10215 (2009).
[40]B. Huang, F. Liu, J. Wu, B.-L. Gu, and W. H. Duan, Phys. Rev. B **77**, 153411 (2008).
[41]X. L. Wang, United States Patent Office, 0042712 (2011).
[42]J. Heyd, G. E. Scuseria, and M. Ernzerhof, J. Chem. Phys. **118**, 8207 (2003).
[43]J. Heyd, G. E. Scuseria, and M. Ernzerhof, J. Chem. Phys. **124**, 219906 (2006).
[44]A. V. Krukau, O. A. Vydrov, A. F. Izmaylov, and G. E. Scuseria, J. Chem. Phys. **125**, 224106 (2006).
[45]S. M. Choi and S. H. Jhi, Phys. Rev. Lett. **101**, 266105 (2008).